SIAM J. APPL. MATH.
Vol. 66, No. 4, pp. 1163–1187

THE EFFECT OF CONTACT LINES ON THE RAYLEIGH INSTABILITY WITH ANISOTROPIC SURFACE ENERGY*

K. F. GURSKI†, G. B. MCFADDEN‡, AND M. J. MIKSIS§

Abstract. We determine the linear stability of a rod or wire on a substrate subject to capillary forces arising from an anisotropic surface energy for a range of contact angles between $-\pi/2$ and $\pi/2$. The unperturbed rod is assumed to have infinite length with a uniform cross-section given by a portion of the two-dimensional equilibrium shape. We examine the effect of surface perturbations on the total energy. The stability of the equilibrium interface is reduced to determining the eigenvalues of a coupled system of ordinary differential equations. This system is solved both asymptotically and numerically for several types of anisotropic surface energies. We find that, in general, the presence of the substrate tends to stabilize the rod.

Key words. Rayleigh instability, contact lines, anisotropic surface energy, quantum wires, nanowires, Plateau

AMS subject classifications. 76E17, 34B24, 34D05, 34D10, 35R35, 65L15, 65L10

DOI. 10.1137/050626946

1. Introduction.

While stability studies of cylindrical rods have a long history, they are still a subject of current interest. For example, nanowires (alternatively called nanorods or quantum wires) are nanoscale crystal structures that are formed by deposition on a substrate, typically with a high lattice-mismatch that tends to produce aligned crystals on the substrate. The processing parameters that govern the growth and stability of the wires are of intense interest. Here we focus on two important issues surrounding nanowire stability: anisotropic surface tension and the contact angle between the rod and substrate.

The analysis of capillary driven instabilities spurring cylindrical rods to break up into droplets was initiated in 1873 by Plateau [27], who showed that breakup will occur when the rod, with isotropic surface energy, is subject to axisymmetric perturbations whose wavelength exceeds the circumference of the cylinder. Lord Rayleigh [28] determined that the length scale of the instability is controlled by the perturbations having the fastest temporal growth rate. The tendency for preferential beading has subsequently become known as the Rayleigh instability. A nice review by Michael may be found in [22]. Molares et al. [23] recently performed an experimental demonstration using the Rayleigh instability of a nanowire to produce long chains of nanospheres.

The surface energy of a liquid-solid or vapor-solid interface is generally anisotropic due to the underlying crystal lattice and depends on the orientation of the local normal

*Received by the editors March 16, 2005; accepted for publication (in revised form) December 15, 2005; published electronically March 24, 2006. The first author was supported by a National Research Council Postdoctoral Fellowship, and the second author was supported by the Microgravity Research Division of NASA. Part of this research was performed at Northwestern University with the support of the NSF Nanoscale Interdisciplinary Research Teams Program under grant DMR-0102794.

http://www.siam.org/journals/siap/66-4/62694.html

†National Institute of Standards and Technology, Gaithersburg, MD 20899-8910. Current address: Department of Mathematics, George Washington University, Washington, DC 20052 (kgurski@gwu.edu).

‡National Institute of Standards and Technology, Gaithersburg, MD 20899-8910 (mcfadden@nist.gov).

§Northwestern University, Department of Engineering Sciences and Applied Mathematics, Evanston, IL 60208 (miksis@northwestern.edu).

vector at each point of the interface [12, 25, 30]. As a first step in applying the analysis of Plateau to a nanowire, the effects of the substrate may be ignored, and the stability of the isolated rod determined strictly by the consideration of anisotropic surface energy. The experimental studies of Kondo and Takayanagi [18] show an apparent stability of elongated nanowires that are grown in a bridge configuration, in contrast to the expected nanoislands or quantum dots predicted by the Rayleigh instability for the isotropic case.

Cahn [2] studied the effect of anisotropic surface energy on the Rayleigh instability for isolated rods with circular cross-sections that are subject to axisymmetric perturbations; the underlying surface free energy was assumed to have transverse isotropy, resulting in closed-form solutions to the stability problem. Glaeser and Stölken [9, 32] extended Cahn's analysis and evaluated the effect of the axisymmetric surface energy anisotropy on evolution kinetics. Gurski and McFadden [10] considered general anisotropic surface energies by computing the second variation of the surface free energy of a freestanding rod whose cross-section is smooth and given by a two-dimensional equilibrium shape. The analysis was applied to examples with uniaxial or cubic anisotropy, which illustrated that anisotropic surface energy plays a significant role in establishing the stability of the rod. It was found that both the magnitude and sign of the anisotropy determine whether the contribution stabilizes or destabilizes the system relative to the case of isotropic surface energy.

Previous theoretical studies of the relationship between the morphological instability of a cylinder that is in contact with a substrate have concentrated on cylinders with isotropic surface energy. McCallum et al. [19] investigated the linear instability of a line of film on a substrate. The unperturbed film state was a cylinder of infinite length with a cross-sectional shape of a segment of a circle. Mass was allowed to flow by diffusion along the film surface. The results of the study found that the substrate presence was a stabilizing influence. Roy and Schwartz [31] studied the stability of liquid ridges on a substrate in the absence of gravity. In this problem the liquid region had a boundary composed of a free surface with a circular arc for a cross-section and a solid cylindrical substrate of arbitrary shape. Their results show that when a particular relationship between the curvatures of the liquid and solid interfaces and the contact angle is satisfied, the infinite liquid ridge is stable with respect to sinuous transverse modes, unlike an infinite cylindrical jet.

For an isotropic surface energy, the base state of the system is relatively simple to describe: the cross-section of the ridge is a circular arc that is determined by the equilibrium contact angles with the substrate. With surface tension anisotropy, the situation is more complicated in several respects. The axis of the nanowire relative to its underlying crystalline axes is a variable to be considered. Once the preferred orientation of the wire axis is established and the wire is assumed to be in contact with the substrate, there remains a geometrical degree of freedom represented by a rotation of the wire about its axis. This rotation exposes different sets of orientations on the crystal-vapor interface, which in turn affects the total energy of the system. Therefore, before the stability to axial perturbations of a nanowire on a substrate is addressed, the selection of the orientation of the wire relative to the substrate must be considered.

During the deposition process, various wire orientations are observed experimentally, depending on the processing conditions and the composition of the deposited crystal and substrate [6, 7, 8, 24, 26, 29]. In particular, for a given set of material parameters, it is argued that the observed orientations depend on kinetics of the (nonequilibrium) deposition process as well as on the effects of surface energy and

surface stress of the crystal-substrate interface [4, 5, 6, 11, 15]. In our simplified model, we consider an inert (nondeforming) substrate with an isotropic crystal-substrate surface energy and ignore kinetic effects by focusing on equilibrium states.

Even with these simplifying assumptions, the identification of the lowest energy orientation of a nanowire on a substrate is more complicated than the simpler problem of determining the lowest energy crystalline orientation of a planar epitaxial layer deposited on a substrate [5, 15, 29], since a nonfacetted nanowire contains a range of crystal-vapor surface orientations instead of the single orientation of a planar film. Within our model, we are able to investigate the low energy orientations of the nanowire on a substrate and perform a stability analysis to axial perturbations (Rayleigh instability).

Our results depend in detail on the anisotropy of the crystal-vapor surface energy. Experimental measurements of this anisotropy for metallic systems are uncommon, although there has been considerable progress recently in atomic-scale simulations of the surface energy anisotropy, specifically for crystal-melt interfaces [1, 14]. Here we adopt a simple one-parameter model for the surface energy anisotropy of the cubic material with a form that is often used to fit the simulation results [1, 14].

In this paper we examine how both the anisotropy of the surface energy of the wire and the interaction of the rod with a substrate affect the stability of the rod. As in the work of Roy and Schwartz [31] on the stability of liquid ridges, we use a variational approach using an energy functional and constant volume condition. Using general anisotropic surface energies, we derive an associated eigenproblem. The eigenproblem is described by a pair of coupled second-order ordinary differential equations with periodic boundary conditions along the axis of the rod and boundary conditions arising from the contact angles between the rod and substrate. We consider the effects of the overall orientation of the crystal relative to the substrate and examine a range of contact angles. The substrate is assumed to be rigid with an isotropic surface energy. We apply the analysis to a number of examples, including the case of a cubic material, and compute the stability of the rod to perturbations when the axis of the rod is aligned parallel to the high symmetry orientations [001], [011], and [111]. When the anisotropy is sufficiently small, the stability of the rod can be computed approximately with asymptotics. For larger levels of anisotropy, the solution is computed numerically.

2. The model. We consider the stability of an infinite rod deposited on a planar substrate below a vapor phase. The rod extends uniformly in the z direction of a Cartesian coordinate system (x, y, z) with the y direction normal to the plane of the substrate. The cross-section of the rod is uniform in z and defined by a two-dimensional equilibrium shape which is determined by surface energy considerations and the angle of contact between crystal and substrate. The vapor-substrate surface energy is denoted by γ_V and the crystal-substrate surface energy is denoted by γ_S. In this model we assume that both γ_V and γ_S are isotropic (constants that are independent of orientation).

Since we will be considering the stability of the rod under an arbitrary shape perturbation, we need to consider the three-dimensional crystal-vapor surface energy for general orientations. The crystal-vapor surface energy will be expressed in terms of the local normal vector to the crystal-vapor interface written in terms of spherical coordinates (ρ, θ, ϕ) in which z is the polar axis, $\rho = \sqrt{x^2 + y^2 + z^2}$ is the radius, θ the polar angle, and ϕ the azimuthal angle as shown in Figure 2.1. The crystal-vapor surface energy is assumed to be anisotropic (orientation-dependent) and is denoted by $\gamma = \gamma(\phi, \theta)$. The unit normal to the unperturbed rod lies in the plane

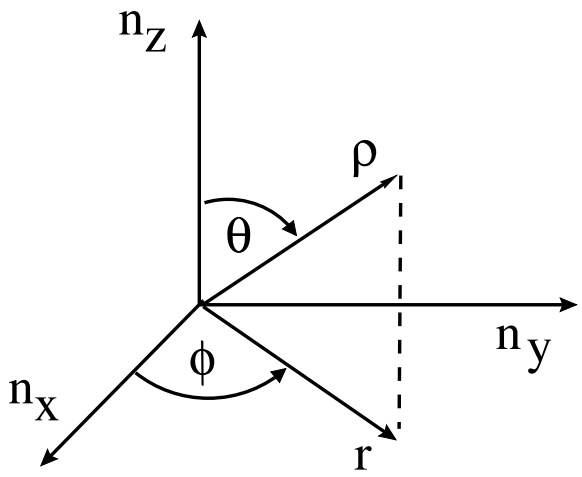

FIG. 2.1. *Schematic diagram of the spherical coordinate system* (ρ, θ, ϕ) *used for the definition of the surface energy* $\gamma(\phi, \theta)$.

$\theta = \pi/2$ and is given by $\hat{\rho}(\phi, \theta = \pi/2) = \hat{r}(\phi) = (\cos\phi, \sin\phi, 0)$, with $\hat{\theta} = -\hat{z}$ and $\hat{\phi}(\phi, \theta = \pi/2) = (-\sin\phi, \cos\phi, 0)$. The axis of the unperturbed rod is parallel to the plane of constant y which represents the substrate. Variables with hats are unit vectors in their corresponding directions.

We restrict our consideration to differentiable surface energies with anisotropies that are mild enough that the surface of the rod is smooth and does not exhibit any missing orientations.

2.1. Three-dimensional surface energy: General formulation. In order to examine the stability of the rod using a variational approach, we will need the general energy functional. This formula and the constant volume condition will be perturbed about the equilibrium rod. The higher order terms in this perturbation expansion will produce a condition for stability. Simply put, for constant volume, if the perturbation increases the energy, the equilibrium state is stable; otherwise it is unstable. This approach parallels the method used by Gurski and McFadden [10], who study the stability of a free rod, but here it is necessary to account for the presence of the substrate.

We will consider the stability of the rod to small amplitude disturbances in the z direction of wavelength $\lambda = 2\pi/k$, where k is the axial wave number. Hence, only the energy and the volume of a portion of the rod of length λ need to be determined. The effect of the substrate on the stability of the rod is local, so only a finite section of the substrate large enough to contain the perturbed rod needs to be examined. In particular, we will consider a rectangular section of the substrate of length λ in the z direction and width $2L_R$ in the x direction.

The total energy of our rod-substrate system, E, can be written as

$$E = E_{CV} + E_{VS} + E_{CS}, \tag{2.1}$$

where E_{CV} is the energy of the crystal-vapor interface, E_{VS} is the energy of the vapor-substrate system, and E_{CS} is the energy of the crystal-substrate system. Letting A_{CS} be the surface area of the crystal-substrate interface, we have that $E_{CS} = \gamma_S A_{CS}$ and $E_{VS} = \gamma_V(2\lambda L_R - A_{CS})$.

The energy of the crystal-vapor interface, E_{CV}, is equal to the surface integral of γ along this interface. If γ is constant, the energy equals γ times the surface area of the crystal-vapor interface. We wish to consider the anisotropic case, so the integral will depend on the orientation of the unit normal to the interface. To compute the associated surface integral, it is helpful to introduce some notation. Let $\vec{X} = \vec{X}(u, v)$ be the position vector of a point along the surface of the rod, where u and v denote surface coordinates. The normal vector field to the rod interface is given by $\vec{P} = \vec{X}_u \times \vec{X}_v$.

Following Gurski and McFadden [10], it is convenient to introduce a generalized surface energy function defined by

$$\Gamma(\vec{P}) = |\vec{P}|\gamma(\Phi, \Theta), \tag{2.2}$$

where

$$\Theta = \tan^{-1}\left(\sqrt{P_x^2 + P_y^2}/P_z\right), \qquad \Phi = \tan^{-1}\left(P_y/P_x\right) \tag{2.3}$$

are the corresponding spherical angles based on the normal vector $\vec{P}$.

A formula for the surface energy can now be obtained by noting that $\gamma(\Phi, \Theta)dA = \Gamma(\vec{P})du\,dv$. The surface energy E_{CV} can therefore be written as

$$E_{CV} = \int\int \Gamma(\vec{P})du\,dv. \tag{2.4}$$

The total energy E is then obtained by substituting (2.4) into (2.1).

It should be noted that the generalized surface energy Γ is closely related to the three-dimensional Cahn–Hoffmann vector [3, 13], $\xi = \nabla\left[\rho\gamma(\phi, \theta)\right]$; in fact,

$$\xi_j(\vec{P}) = \frac{\partial\Gamma(\vec{P})}{\partial P_j}. \tag{2.5}$$

The dimensionless three-dimensional equilibrium shape of a solid particle in a vapor is given by $\vec{\xi}(\phi, \theta)$ for $0 \le \phi \le 2\pi$ and $0 \le \theta \le \pi$, and its normal is $\hat{\rho}(\phi, \theta)$. In the plane $\theta = \pi/2$, this relation reduces to

$$\vec{\xi}(\phi, \pi/2) = \gamma(\phi, \pi/2)\,\hat{r}(\phi) + \gamma_\phi(\phi, \pi/2)\,\hat{\phi}(\phi) - \gamma_\theta(\phi, \pi/2)\,\hat{z}, \tag{2.6}$$

where we have used $\hat{r}(\phi) = (\cos\phi, \sin\phi, 0)$, $\hat{\phi}(\phi) = (-\sin\phi, \cos\phi, 0)$, and $\hat{\theta} = -\hat{z}$ in the plane $\theta = \pi/2$. Note that here partial derivatives are denoted by subscripts, e.g., $\gamma_\phi = \partial\gamma/\partial\phi$. If $\gamma_\theta(\phi, \pi/2) = 0$, then the two-dimensional equilibrium shape defined by (2.6) is characterized by a constant weighted mean curvature $[\gamma + \gamma_{\phi\phi}]\,\mathcal{K}$ [33]. Missing orientations can occur if $\gamma + \gamma_{\phi\phi} < 0$ [35]; here we will assume $\gamma + \gamma_{\phi\phi} > 0$. If $\gamma_\theta(\phi, \pi/2) \neq 0$, then the curve $\vec{\xi}(\phi, \pi/2)$ is out of the plane $z = 0$, but its projection onto the plane represents the two-dimensional equilibrium shape corresponding to $\gamma = \gamma(\phi)$. These two-dimensional shapes define the cross-sections of our rod. We will choose the surface coordinates $(u, v) = (\phi, z)$, which is a natural choice for studying the stability of the equilibrium rod along a substrate to small perturbations.

2.2. The equilibrium rod. The cross-section of the unperturbed rod is a portion of a two-dimensional equilibrium shape parameterized by the vector $\vec{X}^{(0)}(\phi) = (X^{(0)}(\phi), Y^{(0)}(\phi))$, where

$$X^{(0)}(\phi) = \frac{\ell}{\gamma_0}\left[\gamma\left(\phi, \frac{\pi}{2}\right)\cos\phi - \gamma_\phi\left(\phi, \frac{\pi}{2}\right)\sin\phi\right] \tag{2.7}$$

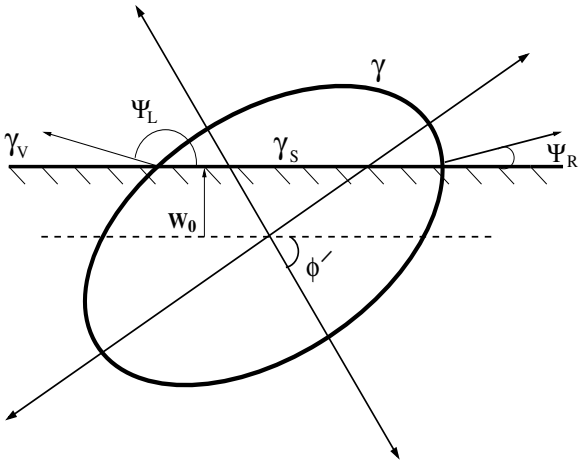

FIG. 2.2. *Ellipse rotated an angle of ϕ' about the original axes. Contact angles between the ellipse and substrate are ψ_R and ψ_L.*

and

$$Y^{(0)}(\phi) = \frac{\ell}{\gamma_0}\left[\gamma\left(\phi, \frac{\pi}{2}\right)\sin\phi + \gamma_\phi\left(\phi, \frac{\pi}{2}\right)\cos\phi\right] \tag{2.8}$$

for $\psi_R \le \phi \le \psi_L$, where $\gamma(\phi,\theta)$ is the surface energy, ℓ is a characteristic length scale, and γ_0 is a characteristic surface energy (see, e.g., [35]). Anticipating the subsequent perturbation expansion, we associate variables having a superscript (0) with the equilibrium rod. The rod is in contact with the substrate over the range $X^{(0)}(\psi_L) \le x \le X^{(0)}(\psi_R)$, and the surface of the substrate in this coordinate system is $y = W_0 = Y^{(0)}(\psi_R) = Y^{(0)}(\psi_L)$. The contact angle that the rod makes with the substrate thus is described by ψ_R and ψ_L, as illustrated in Figure 2.2. Winterbottom [36] (see also [3]) shows that the conditions for equilibrium at the contact line are satisfied for the choice $W_0 = (\ell/\gamma_0)[\gamma_V - \gamma_S]$; we also derive this result below in the course of the energy minimization. Unless otherwise noted, we will henceforth assume that all variables are dimensionless, based on the units of length ℓ and energy γ_0.

3. Stability under perturbations. We determine the stability of the rod by computing the total energy of a volume-preserving perturbation to the rod. The unperturbed interface can be written in the form $\vec{X}^{(0)}(\phi) + z\,\hat{z}$. As in our previous development (see [10]), we then consider a perturbed interface of the form

$$\vec{X}(\phi, z) = \vec{X}^{(0)}(\phi) + z\,\hat{z} + \epsilon h(\phi, z)\hat{r}(\phi) + \frac{\epsilon^2}{2}h_2\hat{r}(\phi) + \cdots, \tag{3.1}$$

where ϵ is a small parameter, $h(\phi, z)$ is the height of the perturbation along the normal $\hat{r}$ to the unperturbed shape, and the constant h_2 is a second-order shape correction introduced to satisfy the volume constraint at $O(\epsilon^2)$. The domain of ϕ is given by $\psi_R(z) \le \phi \le \psi_L(z)$. Note that the contact angles depend on both z and ϵ since the contact angles are determined by the boundary conditions at the contact point. In particular, we will assume that ψ_i has a regular expansion in ϵ of the form

$$\psi_i(z) = \psi_i^{(0)} + \epsilon\psi_i^{(1)}(z) + \frac{\epsilon^2}{2}\psi_i^{(2)}(z) + \cdots \tag{3.2}$$

for $i = L, R$. At the substrate we have

$$Y(\psi_i, z) = W_0, \tag{3.3}$$

so that at leading order we have

$$W_0 = Y^{(0)}(\psi_i^{(0)}) = \gamma(\psi_i^{(0)}, \pi/2)\sin\psi_i^{(0)} + \gamma_\phi(\psi_i^{(0)}, \pi/2)\cos\psi_i^{(0)} \tag{3.4}$$

for $i = L, R$. The case $W_0 = 0$, $\psi_R^{(0)} = 0$, $\psi_L^{(0)} = \pi$ represents a contact line at the orientation of an equatorial plane of symmetry of the equilibrium shape and also corresponds to the upper half of a freely suspended rod [10].

At the contact line the variables X, Y, h, and ψ are related through (3.1)–(3.3). Expanding (3.3) to first order yields

$$Y_\phi^{(0)}(\psi_i^{(0)})\psi_i^{(1)} + Y^{(1)}(\psi_i^{(0)}, z) = 0, \tag{3.5}$$

where from (3.1) the first-order shape change is given by

$$X^{(1)}(\phi, z) = h(\phi, z)\cos\phi, \quad Y^{(1)}(\phi, z) = h(\phi, z)\sin\phi. \tag{3.6}$$

Since $X_\phi^{(0)}(\psi_i^{(0)}) = -(\gamma+\gamma_{\phi\phi})\sin\psi_i^{(0)}$ and $Y_\phi^{(0)}(\psi_i^{(0)}) = (\gamma+\gamma_{\phi\phi})\cos\psi_i^{(0)}$, (3.5) yields

$$\psi_i^{(1)}(z) = \frac{-h(\psi_i^{(0)}, z)\sin\psi_i^{(0)}}{(\gamma + \gamma_{\phi\phi})\cos\psi_i^{(0)}}, \tag{3.7}$$

which relates h and $\psi^{(1)}$ at the contact line.

The geometry of the perturbed rod is determined by the two tangent vectors $\vec{X}_\phi$ and $\vec{X}_z$, and their cross product, $\vec{P} = \vec{X}_\phi \times \vec{X}_z$, which is normal to the interface. The area element on the interface is given by $dA = |\vec{P}|\, d\phi\, dz$. Evaluating the tangent vectors by using (3.1) and taking their cross product, we find that the interface normal has the expansion

$$\vec{P}(\phi, z) = \vec{P}^{(0)}(\phi) + \epsilon\vec{P}^{(1)}(\phi, z) + \frac{\epsilon^2}{2}\vec{P}^{(2)}(\phi, z) + O(\epsilon^3), \tag{3.8}$$

where

$$\vec{P}^{(0)} = (\gamma + \gamma_{\phi\phi})\,\hat{r}, \tag{3.9}$$

$$\vec{P}^{(1)} = h\,\hat{r} - h_\phi\,\hat{\phi} - (\gamma + \gamma_{\phi\phi})\,h_z\,\hat{z}, \tag{3.10}$$

$$\vec{P}^{(2)} = h_2\,\hat{r} - 2hh_z\,\hat{z}. \tag{3.11}$$

3.1. Volume. The shape perturbation (3.1) is required to preserve the volume of the rod over a given length with a period of the perturbation equal to $\lambda = 2\pi/k$. As in Gurski and McFadden [10], we can write the volume as a surface integral by using the divergence theorem. Then using the expansion (3.1), we find that to $O(\epsilon^2)$ the volume is given by

$$\begin{aligned} V &= \frac{1}{2}\int\int\int \nabla\cdot(x, y, 0)\, dV \\ &= \frac{1}{2}\int_0^{2\pi/k}\int_{\psi_R(z)}^{\psi_L(z)} \vec{P}(\phi, z)\cdot[\vec{X}(\phi, z) - z\,\hat{z}]\, d\phi\, dz \end{aligned} \tag{3.12}$$

$$
\begin{aligned}
&-\frac{1}{2}\int_0^{2\pi/k} W_0\left[X(\psi_R(z),z)-X(\psi_L(z),z)\right]\,dz \\
&=\frac{1}{2}\int_0^{2\pi/k}\int_{\psi_R(z)}^{\psi_L(z)}\left\{\left[\gamma+\epsilon h+\frac{\epsilon^2}{2}h_2\right]\left[(\gamma+\gamma_{\phi\phi})+\epsilon h+\frac{\epsilon^2}{2}h_2\right]-\epsilon\gamma_\phi h_\phi\right\}d\phi\,dz \\
&\quad-\frac{1}{2}\int_0^{2\pi/k} W_0\left[X(\psi_R(z),z)-X(\psi_L(z),z)\right]\,dz.
\end{aligned}
$$

Expanding in ϵ then gives

$$V = V^{(0)} + \epsilon V^{(1)} + \frac{\epsilon^2}{2}V^{(2)} + O(\epsilon^3) + \cdots, \tag{3.13}$$

where

$$V^{(0)} = \frac{\lambda}{2}\int_{\psi_R^{(0)}}^{\psi_L^{(0)}} \gamma\left(\gamma+\gamma_{\phi\phi}\right)\,d\phi - \frac{\lambda}{2}W_0[X^{(0)}(\psi_R^{(0)}) - X^{(0)}(\psi_L^{(0)})], \tag{3.14}$$

$$V^{(1)} = \int_0^{2\pi/k}\int_{\psi_R^{(0)}}^{\psi_L^{(0)}} h\left(\gamma+\gamma_{\phi\phi}\right)\,d\phi\,dz, \tag{3.15}$$

$$V^{(2)} = \int_0^{2\pi/k}\int_{\psi_R^{(0)}}^{\psi_L^{(0)}} \left\{h^2 + h_2\left(\gamma+\gamma_{\phi\phi}\right)\right\}d\phi\,dz - \int_0^{2\pi/k} h^2\tan\phi\Big|_{\psi_R^{(0)}}^{\psi_L^{(0)}}\,dz. \tag{3.16}$$

A perturbation $h(\phi,z)$ that is periodic in z with mean zero makes $V^{(1)}=0$, and the condition $V^{(2)}=0$ then determines the appropriate value of the constant h_2. A perturbation $h(\phi)$ that is independent of z does not automatically make $V^{(1)}=0$. This represents a special case for the stability calculation that is treated in the appendix.

3.2. Energy. The stability of the rod is determined by expanding the total energy through $O(\epsilon^2)$ for $|\epsilon| \ll 1$, and, for a given volume, examining whether the shape perturbation, constrained to maintain constant volume of the rod, raises or lowers the energy of the rod. Since the rod is assumed to be infinite in the z direction, an analysis in terms of Fourier components allows us to consider shape perturbations that are periodic in z. The contact angle is now a function of z as well, $\psi_i = \psi_i(z)$ for both $i = L, R$, and the energy E in the region $-L < x < L$ and $0 < z < 2\pi/k$ from (2.1) is given by

$$
\begin{aligned}
E = &\int_0^{2\pi/k} dz \int_{\psi_R(z)}^{\psi_L(z)} \Gamma(\vec{P}(\phi,z))\,d\phi + \frac{4\pi\gamma_V L_R}{k} \\
&-(\gamma_V-\gamma_S)\int_0^{2\pi/k}\left[X(\psi_R(z),z)-X(\psi_L(z),z)\right]dz.
\end{aligned} \tag{3.17}
$$

Expanding in powers of ϵ, we find

$$E = E^{(0)} + \epsilon E^{(1)} + \frac{\epsilon^2}{2}E^{(2)} + O(\epsilon^3), \tag{3.18}$$

where

$$E^{(0)} = \int_0^{2\pi/k} dz \int_{\psi_R^{(0)}}^{\psi_L^{(0)}} \gamma\left(\gamma + \gamma_{\phi\phi}\right)\, d\phi + \frac{4\pi\gamma_V L}{k} + \left(\gamma_V - \gamma_S\right) \int_0^{2\pi/k} \left(\gamma\cos\phi - \gamma_\phi \sin\phi\right) \Big|_{\psi_R^{(0)}}^{\psi_L^{(0)}} dz. \tag{3.19}$$

The first variation of the energy is

$$\frac{E^{(1)}}{2} = \int_0^{2\pi/k} dz \int_{\psi_R^{(0)}}^{\psi_L^{(0)}} \left\{(\gamma + \gamma_{\phi\phi})h + \gamma_\theta\left(\gamma + \gamma_{\phi\phi}\right) h_z\right\} d\phi - \int_0^{2\pi/k} dz \left(\frac{h(\phi, z)}{\cos\phi}\left\{[\gamma_S - \gamma_V] + [\gamma\sin\phi + \gamma_\phi\cos\phi]\right\}\right) \Big|_{\psi_R^{(0)}}^{\psi_L^{(0)}}, \tag{3.20}$$

where we used (3.7) to simplify the second integral.

The second variational term is

$$\begin{aligned}\frac{E^{(2)}}{2} = &\int_0^{2\pi/k} dz \int_{\psi_R^{(0)}}^{\psi_L^{(0)}} \left[h_\phi^2 + (\gamma + \gamma_{\phi\phi})(\gamma + \gamma_{\theta\theta})h_z^2 - 2\gamma_{\phi\theta}h_\phi h_z + \gamma h_2 + 2\gamma_\theta h h_z\right] d\phi \\ &+ \int_0^{2\pi/k} \left\{\left[h_2\gamma_\phi(\psi_L^{(0)}) - 2\gamma_\theta(\psi_L^{(0)})h(\psi_L^{(0)}, z)h_z(\psi_L^{(0)}, z)\tan\psi_L^{(0)}\right]\right. \\ &\left. - \left[h_2\gamma_\phi(\psi_R^{(0)}) - 2\gamma_\theta(\psi_R^{(0)})h(\psi_R^{(0)}, z)h_z(\psi_R^{(0)}, z)\tan\psi_R^{(0)}\right]\right\} dz.\end{aligned} \tag{3.21}$$

3.3. Three-dimensional eigenvalue problem. Our choice of $h(\phi, z)$ makes the integral of the sum of the second and fourth terms in (3.21) identically zero. Eliminating h_2 from (3.21) by using the volume condition, $V^{(2)} = 0$ in (3.16), and integrating by parts, we find that

$$\begin{aligned}\frac{E^{(2)}}{2} = &-\int_0^{2\pi/k} dz \int_{\psi_R^{(0)}}^{\psi_L^{(0)}} h\mathcal{L}h\, d\phi \\ &+ \int_0^{2\pi/k} \left\{\left[h(\psi_L^{(0)}, z)\tan\psi_L^{(0)} + h_\phi(\psi_L^{(0)}, z) - \gamma_{\theta\phi}(\psi_L^{(0)})h_z(\psi_L^{(0)}, z)\right]h(\psi_L^{(0)}, z)\right. \\ &\left. - \left[h(\psi_R^{(0)}, z)\tan\psi_R^{(0)} + h_\phi(\psi_R^{(0)}, z) - \gamma_{\theta\phi}(\psi_R^{(0)})h_z(\psi_R^{(0)}, z)\right]h(\psi_R^{(0)}, z)\right\} dz,\end{aligned} \tag{3.22}$$

where

$$\mathcal{L}h = h_{\phi\phi} + (\gamma + \gamma_{\phi\phi})(\gamma + \gamma_{\theta\theta})h_{zz} - \gamma_{\phi\theta}h_{\phi z} - \left(\gamma_{\theta\phi}h_z\right)_\phi + h. \tag{3.23}$$

Recall that the aim of this calculation is to determine perturbations h such that $E^{(2)} > 0$. This condition can be satisfied if the eigenvalue problem

$$\mathcal{L}h = \mu h \tag{3.24}$$

with boundary conditions

$$h(\psi_i^{(0)}, z)\sin\psi_i^{(0)} + h_\phi(\psi_i^{(0)}, z)\cos\psi_i^{(0)} - \gamma_{\theta\phi}(\psi_i^{(0)})h_z(\psi_i^{(0)}, z)\cos\psi_i^{(0)} = 0 \tag{3.25}$$

for $i = L, R$ has only negative eigenvalues μ. The differential operator $\mathcal{L}$ is identical to that for the isolated rod as given in [10], but instead of periodicity in ϕ we now have boundary conditions that apply at $\psi_R^{(0)}$ and $\psi_L^{(0)}$.

Assuming a discrete set of eigenvalues μ_n and eigenfunctions h_n, for $n = 0, 1, 2, \ldots$, we can rewrite the eigenvalue problem (3.24)–(3.25) as

$$\partial_{\phi\phi}h_n + (\gamma + \gamma_{\phi\phi})(\gamma + \gamma_{\theta\theta})\partial_{zz}h_n - \gamma_{\phi\theta}\partial_{\phi z}h_n - (\gamma_{\theta\phi}\partial_z h_n)_\phi + h_n = \mu_n h_n, \tag{3.26}$$

where the eigenfunctions h_n satisfy the boundary conditions given by (3.25) for $i = L, R$. Note that (3.26) must also satisfy periodicity in the z direction, which can be satisfied by assuming the solution has the form $h_n(\phi, z) = H_n(\phi)\sin kz + G_n(\phi)\cos kz$. Substituting this into (3.26) implies

$$\frac{d^2H_n}{d\phi^2} + (1 - k^2(\gamma + \gamma_{\phi\phi})(\gamma + \gamma_{\theta\theta}))H_n + k\gamma_{\phi\theta}\frac{dG_n}{d\phi} + k\left(\gamma_{\theta\phi}G_n\right)_\phi = \mu_n H_n, \tag{3.27}$$

$$\frac{d^2G_n}{d\phi^2} + (1 - k^2(\gamma + \gamma_{\phi\phi})(\gamma + \gamma_{\theta\theta}))G_n - k\gamma_{\phi\theta}\frac{dH_n}{d\phi} - k\left(\gamma_{\theta\phi}H_n\right)_\phi = \mu_n G_n \tag{3.28}$$

with the boundary conditions

$$H_n \sin\psi_i^{(0)} + \frac{dH_n}{d\phi}\cos\psi_i^{(0)} + k\gamma_{\theta\phi}(\psi_i^{(0)})G_n\cos\psi_i^{(0)} = 0, \tag{3.29}$$

$$G_n \sin\psi_i^{(0)} + \frac{dG_n}{d\phi}\cos\psi_i^{(0)} - k\gamma_{\theta\phi}(\psi_i^{(0)})H_n\cos\psi_i^{(0)} = 0 \tag{3.30}$$

for $i = L, R$. This coupled system of equations must be solved to determine the eigenfunctions and eigenvalues. Note that if γ is independent of θ, the equations decouple.

4. Rotation and contact angles. In the next two sections we consider two related aspects of the stability of a two-dimensional rod on a substrate. We first consider the preferred, low energy orientations of the two-dimensional rod neglecting axial perturbations. For this evaluation, we fix the rod axis that lies parallel to the substrate and compute the energy of the system as the rod is rotated about this axis. Given the specification of the axis of the rod, we assume that preferred orientations correspond to minima of the energy as a function of the rotation angle. Once the low energy orientations are determined, we go on to consider the further effect of axial perturbations on the stability of rods aligned in the preferred orientation.

4.1. Ellipse. Consider the special case of a rod whose cross-section is given by a two-dimensional ellipse,

$$\frac{x^2}{a_x^2} + \frac{y^2}{a_y^2} = 1. \tag{4.1}$$

The major and minor axes of the ellipse are then rotated with respect to the x-axis by an angle ϕ', as shown in Figure 2.2. The corresponding surface free energy γ is given by

$$\gamma(\phi) = \sqrt{a_x^2\cos^2(\phi + \phi') + a_y^2\sin^2(\phi + \phi')}. \tag{4.2}$$

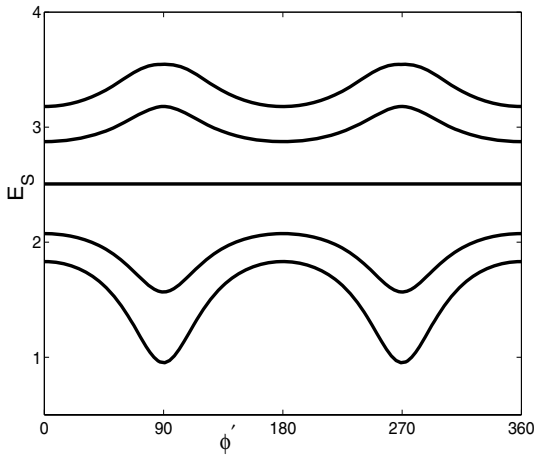

FIG. 4.1. *Scaled energy versus rotation angle for the ellipse. From the top at* $\phi' = 0$ *the curves correspond to* $\tilde{W}_0 = -1.0, -0.5, 0, 0.5, 0.75$.

The surface of the substrate is the plane $y = W_0 = (\gamma_V - \gamma_S)$, and the ellipse makes contact with the substrate with two angles ψ_R and ψ_L, which are roots of the equation

$$0 = W_0 - [\gamma(\phi)\sin\phi + \gamma_\phi(\phi)\cos\phi]. \tag{4.3}$$

If ϕ' is zero or $\pi/2$, then $\psi_L = \pi - \psi_R$.

First, let us consider how the energy depends on the angle of rotation ϕ' and the parameter W_0. Since the volume of a rod with an elliptical cross-section will vary as W_0 varies, we must find a normalization for the energy

$$E = \lambda \int_{\psi_R}^{\psi_L} \gamma\,(\gamma + \gamma_{\phi\phi})\; d\phi - \lambda W_0\,(X(\psi_R) - X(\psi_L)) + 2\lambda L\gamma_V. \tag{4.4}$$

The corresponding formula for the volume of the rod is

$$V = \frac{\lambda}{2} \int_{-\pi/2}^{3\pi/2} \gamma\,(\gamma + \gamma_{\phi\phi})\; d\phi - \lambda \int_{\psi_L}^{\psi_R+2\pi} (W_0 - Y)\; \frac{\partial X(\phi)}{\partial \phi}\, d\phi. \tag{4.5}$$

Using these definitions, we can define a normalized energy E_S as

$$E_S = \frac{E - 2L\gamma_V}{\sqrt{2V\lambda}} = \frac{\int_{\psi_R}^{\psi_L} \gamma\,(\gamma + \gamma_{\phi\phi})\; d\phi - W_0\,(X(\psi_R) - X(\psi_L))}{\sqrt{\int_{-\pi/2}^{3\pi/2} \gamma\,(\gamma + \gamma_{\phi\phi})\; d\phi - 2\int_{\psi_L}^{\psi_R+2\pi} (W_0 - Y)\; \frac{\partial X(\phi)}{\partial \phi}\, d\phi}}. \tag{4.6}$$

For our numerical calculations we set $a_x = 1$, $a_y = 2$. Figure 4.1 shows that when $W_0 > 0$, the lowest scaled energy E_S is attained when $\phi' = 90$ (i.e., the major axis is horizontal) and the highest scaled energy is reached when $\phi' = 0$ degrees (i.e., the major axis is vertical). Since $W_0 = \gamma_V - \gamma_S > 0$, the lowest energy state of the ellipse will be where contact between the crystal and the substrate is maximized and where contact between the substrate and vapor is minimized, i.e., when the semimajor axis is horizontal. The scaled energy is independent of ϕ' when W_0 is zero, showing that when $\gamma_V = \gamma_S$, there is no preferred rod orientation. When W_0 is negative, the scaled energy is higher at $\phi' = 90$ degrees and lower at $\phi' = 0$ degrees as the crystal orients itself to minimize the crystal-substrate interface.

4.2. Cubic materials. A simple model of the surface energy anisotropy for a cubic material is given by the dimensionless expression [20]

$$\gamma(n'_x, n'_y, n'_z) = \left\{1 + 4\epsilon_4([n'_x]^4 + [n'_y]^4 + [n'_z]^4)\right\}, \tag{4.7}$$

where we employ a primed coordinate system that is attached to the crystal axes. We will consider rod directions z that coincide with the high symmetry orientations [001], a fourfold axis; [011], a twofold axis; and [111], a threefold axis. We will use appropriate preliminary rotations of the crystal axes in each case to bring these axes into alignment with the z-axis of the rod, which will be fixed in the unprimed coordinate system.

The shapes are smooth for $-1/18 < \epsilon_4 < 1/12$ (see [20]). For $\epsilon_4 < 0$ the shapes resemble rounded cubes, with [110] edges first forming at $\epsilon_4 = -1/18 \approx -0.0556$. As ϵ_4 decreases below $-1/18$, the edges extend toward the [111] directions, merging to form a corner for $\epsilon_4 = -5/68 \approx -0.07735$. For $\epsilon_4 > 0$ the shapes are octahedral, with [100] corners first forming at $\epsilon_4 = 1/12 \approx 0.0833$.

4.2.1. Rod axis parallel to [001] orientation. If the axis of the rod is aligned with the [001] orientation of the crystal, the dimensionless surface energy resulting from (4.7) is given by [16, 17, 21]

$$\gamma(\phi, \theta) = 1 + \epsilon_4 \left[4\cos^4\theta + \sin^4\theta\,(3 + \cos 4\phi)\right]. \tag{4.8}$$

In the plane $\theta = \pi/2$,

$$\gamma = (1 + 3\epsilon_4) + \epsilon_4 \cos 4\phi. \tag{4.9}$$

If we allow the crystal to rotate on the substrate, we must include the effect of the rotation angle ϕ',

$$\gamma = (1 + 3\epsilon_4) + \epsilon_4 \cos 4\,(\phi + \phi'). \tag{4.10}$$

We can determine the scaled energies using (4.6). Results are shown in Figure 4.2 for several values of ϵ_4 in the range of -0.0556 to 0.0833. The two extreme heights of $W_0 = \pm W_M$, where

$$W_M = \min\left(0.95\sqrt{X(0)^2 + Y(0)^2}, 0.95\sqrt{X(\pi/2)^2 + Y(\pi/2)^2}\right), \tag{4.11}$$

are shown. When W_0 is near $-W_M$, i.e., the origin of the coordinate system is nearly at a maximum height above the substrate surface, the effects of rotation are very slight, with maxima at $\phi' = 0$, 90, 180, 270, and 360 degrees for negative ϵ_4. When ϵ_4 is positive, these maxima switch to minima. The plot of the scaled energy versus angle of rotation for $\epsilon_4 = -0.0556$ has the largest oscillations with an amplitude of 0.001. The fourfold symmetry of the [001] oriented crystal is responsible for the 90 degree spacing. When W_0 is near W_M, the location of the maxima and minima reverse with respect to their locations at $W_0 = -W_M$, and the effect of the rotation becomes more pronounced.

4.2.2. Rod axis parallel to [011] orientation. If the axis of the rod is aligned with the [011] orientation of the crystal, then an appropriate rotation of the crystal axes relative to the rod axis is given by [20]

$$\begin{pmatrix} n'_x \\ n'_y \\ n'_z \end{pmatrix} = \begin{pmatrix} 1 & 0 & 0 \\ 0 & 1/\sqrt{2} & 1/\sqrt{2} \\ 0 & -1/\sqrt{2} & 1/\sqrt{2} \end{pmatrix} \begin{pmatrix} n_x \\ n_y \\ n_z \end{pmatrix}. \tag{4.12}$$

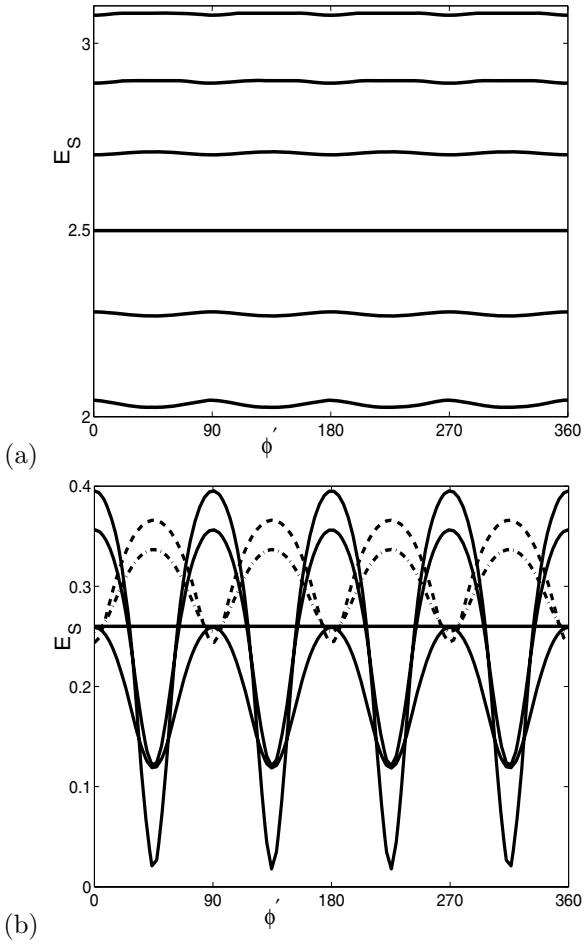

FIG. 4.2. *Scaled energy versus ϕ' for the* [001] *cubic orientation.* (a) *From the bottom, the curves are* $\epsilon_4 = -0.0556,\ -0.02778,\ 0.0,\ 0.02778,\ 0.0556,\ 0.0833$. $W_0 = -W_M$. (b) *From the top, the two dashed curves are* $\epsilon_4 = -0.0556$ *and* -0.02778, *and the solid curves are* $\epsilon_4 = 0.0,\ 0.02778,\ 0.0556,\ 0.0833$. $W_0 = W_M$.

This rotation gives

$$\gamma = 1 + 4\epsilon_4 \left(n_x^4 + \frac{n_y^4}{2} + \frac{n_z^4}{2} + 3n_y^2 n_z^2 \right), \tag{4.13}$$

which reduces to

$$\gamma = 1 + 2\epsilon_4 \left(\cos^4\theta + 6\cos^2\theta \sin^2\theta \sin^2\phi + 2\sin^4\theta \cos^4\phi + \sin^4\theta \sin^4\phi \right). \tag{4.14}$$

When $\theta = \pi/2$ and rotation of the crystal about the substrate is included, then

$$\gamma = 1 + \epsilon_4 \left[\frac{9}{4} + \cos 2(\phi + \phi') + \frac{3}{4} \cos 4(\phi + \phi') \right]. \tag{4.15}$$

The rod is smooth for $-5/68 \le \epsilon_4 \le 1/12$, which is a larger range than the [001] case.

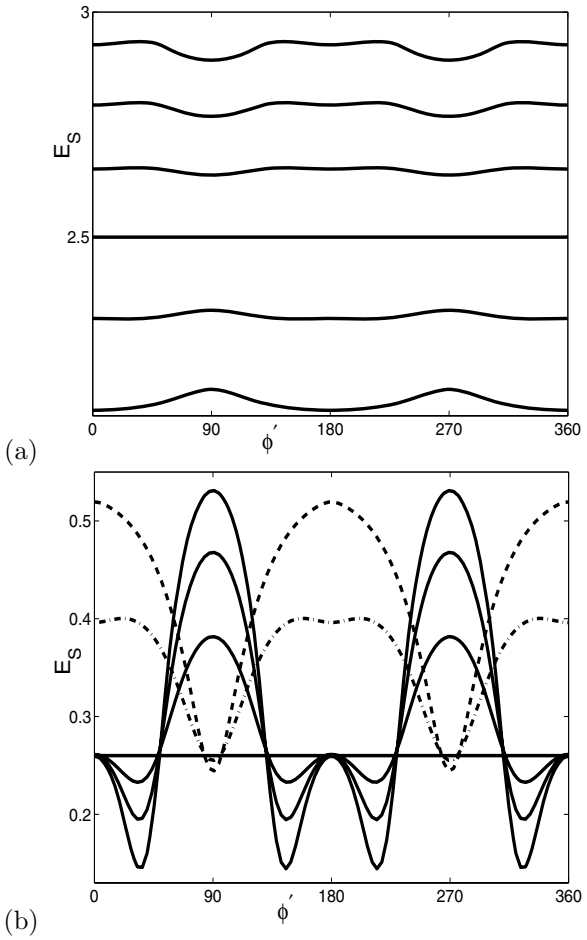

FIG. 4.3. *Scaled energy versus θ' for the* [011] *cubic orientation.* (a) *From the bottom, the curves are* $\epsilon_4 = -0.0556, -0.02778, 0.0, 0.02778, 0.0556, 0.0833$. $\tilde{W}_0 = -W_{M'}$. (b) *At* $\theta' = 0$ *from the bottom, the two dashed curves correspond to* $\epsilon_4 = -0.0556$ *and* -0.02778*, and the solid curves correspond to* $\epsilon_4 = 0.0, 0.02778, 0.0556, 0.0833$. $\tilde{W}_0 = W_M$.

We can determine the scaled energies using (4.6). Results are shown in Figure 4.3 for several values of ϵ_4 in the range of -0.0556 to 0.0833 for the two extreme heights of $W_0 = \pm W_M$. The twofold symmetry of the [011] crystal is apparent in the spacing of maxima and minima shown in Figure 4.3. When ϵ_4 is negative, the minima (maxima) are located at 0, 180, and 360 degrees for $W_0 = -W_M(+W_M)$. When ϵ_4 is positive, the minima are located at 90 and 270 degrees for $W_0 = -W_M$. At $W_0 = W_M$, maxima are maintained at 90 and 270 degrees for positive ϵ_4. We see that secondary local maxima form at $\phi' = 0$, 180, 360 for positive ϵ_4 at $W_0 = W_M$.

4.2.3. Rod axis parallel to [111] orientation. If the axis of the rod is aligned with the [111] orientation of the crystal, then an appropriate rotation of the crystal axes relative to the rod axis is given by [20]

$$\begin{pmatrix} n'_x \\ n'_y \\ n'_z \end{pmatrix} = \begin{pmatrix} \sqrt{2}/\sqrt{3} & 0 & 1/\sqrt{3} \\ -1/\sqrt{6} & 1/\sqrt{2} & 1/\sqrt{3} \\ -1/\sqrt{6} & -1/\sqrt{2} & 1/\sqrt{3} \end{pmatrix} \begin{pmatrix} n_x \\ n_y \\ n_z \end{pmatrix}. \tag{4.16}$$

This leads to the form

$$\gamma = 1 + 4\epsilon_4\left(\frac{n_x^4}{2} + \frac{n_y^4}{2} + \frac{n_z^4}{3} + n_x^2 n_y^2 + 2n_x^2 n_z^2 + 2n_y^2 n_z^2 + \frac{2\sqrt{2}}{3} n_x^3 n_z - 2\sqrt{2} n_x n_y^2 n_z\right), \tag{4.17}$$

which reduces to

$$\gamma = 1 + 4\epsilon_4\left(\frac{1}{3}\cos^4\theta + 2\cos^2\theta\sin^2\theta + \frac{1}{2}\sin^4\theta + \frac{2\sqrt{2}}{3}\cos\theta\sin^3\theta\cos 3\phi\right). \tag{4.18}$$

Although the [111] orientation is not isotropic, in the $\theta = \pi/2$ plane,

$$\gamma = 1 + 2\epsilon_4. \tag{4.19}$$

Therefore, the effect of the ϕ dependence is lost and the surface energy for the [111] orientation is unchanged by a rotation of ϕ' about the substrate.

5. Linear stability calculations. Next we investigate the linear stability of the system by examining the eigenvalue problem associated with diagonalizing the second variation of the energy for a fixed orientation of the rod on the substrate. We consider a number of examples, including an ellipsoidal surface energy anisotropy and several variants of cubic anisotropy. The three-dimensional study includes both numerical and asymptotic results. A discussion on the effect of rotation on stability is covered in the appendix.

5.1. Ellipsoidal anisotropy. We first discuss an anisotropic surface energy that leads to an ellipsoidal equilibrium shape described by

$$\frac{x^2}{a_x^2} + \frac{y^2}{a_y^2} + \frac{z^2}{a_z^2} = 1. \tag{5.1}$$

We consider an axisymmetric shape with $a_x = a_y = 1$. The corresponding surface free energy is given by $\gamma(\phi,\theta) = \sqrt{\sin^2\theta + a_z^2\cos^2\theta}$, and in the plane $\theta = \pi/2$ we have $\gamma = 1$, $\gamma_{\phi\phi} = 0$, $\gamma_{\theta\phi} = 0$, and $\gamma_{\theta\theta} = a_z^2 - 1$. The eigenvalue problem (3.27)–(3.28) decouples, leading to the single equation

$$\frac{\partial^2 H_n}{\partial\phi^2} + (1 - K^2)H_n = \mu_n H_n, \tag{5.2}$$

where $K = a_z k$. The boundary conditions for $i = L, R$ are

$$H_n(\psi_i^{(0)})\sin\psi_i^{(0)} + H_{n\phi}(\psi_i^{(0)})\cos\psi_i^{(0)} = 0. \tag{5.3}$$

We solve this problem numerically using a pseudospectral Chebyshev method for a range of contact angles determined by solutions to (4.3), where $-1 \le W_0 \le 1$. To eliminate the change in length scale with the contact angle, we define $\kappa = KR_e$ as the dimensionless axial wave number based on the effective radius of the cross-section.

In Figure 5.1(a) we show the most unstable mode μ_0 for a range of contact angles ψ_R as a function of κ. The results indicate that the ellipsoid is stabilized with respect to long wavelengths for large ψ_R. In Figure 5.1(b) we plot the square of the critical wavenumber κ_C, which corresponds to the transition between stable and unstable behavior, as a function of the contact angle ψ_R.

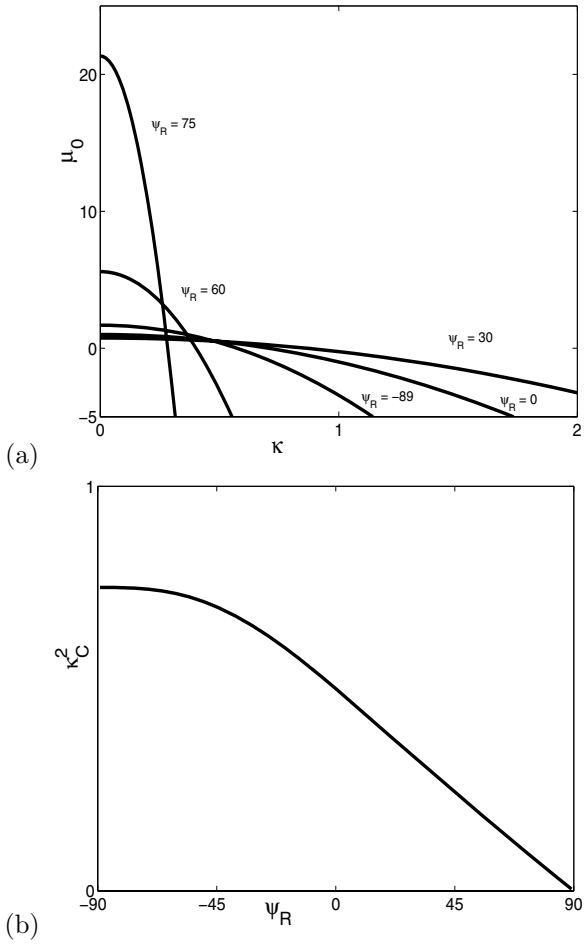

FIG. 5.1. (a) *Eigenvalues for $n = 0$ versus $\kappa = R_e K$ for the ellipsoid case. From the lower curve at $\kappa = 0$: $\psi_R^{(0)} = -89, 0, 30, 60, 75$ degrees.* (b) *The square of the rescaled wave number, κ_C^2, versus ψ_R for the ellipsoid.*

5.2. Cubic materials. For numerical determination of the eigenvalues we used a pseudospectral Chebyshev discretization of the (3.27), (3.28) with boundary conditions from (3.25) for contact angles, where $-\pi \leq \psi_R \leq \pi$. For this problem we may choose a value ψ_R, thereby fixing the value of W_0. If we restrict ψ_R between $-\pi/2$ and $\pi/2$, then ψ_L is the solution to

$$W_0 - (\gamma(\phi)\sin\phi + \gamma_\phi(\phi)\cos\phi) = 0 \tag{5.4}$$

for a value of ϕ between $\pi/2$ and $3\pi/2$. Therefore, fixing the value of ψ_R determines the value of ψ_L.

Since γ varies with respect to ϵ_4 for each of the three high symmetry cubic orientations [001], [011], and [111], we must determine the effective radius of the cross-section R_e. To eliminate the change in length scale with ϵ_4, we set $\kappa = kR_e$, which is the dimensionless axial wave number based on the effective radius of the cross-section.

In addition, we performed an asymptotic expansion of the problem with a plane of symmetry at $\phi = \pi/2$, i.e., when $\psi_L = \pi - \psi_R$. The results for the numerical cal-

culation will be compared to the results for the asymptotic expansion in the following sections.

5.2.1. Rod axis parallel to [001] orientation. The dimensionless surface energy is given by (4.8) for the [001] orientation. In the plane $\theta = \pi/2$, we then have $\gamma_{\theta\phi} = 0$, and

$$\gamma = (1 + 3\epsilon_4) + \epsilon_4 \cos 4\phi, \tag{5.5}$$

$$(\gamma + \gamma_{\phi\phi})(\gamma + \gamma_{\theta\theta}) = \left(1 - 6\epsilon_4 - \frac{9}{2}\epsilon_4^2\right) - (18\epsilon_4 - 126\epsilon_4^2)\cos 4\phi + \frac{45}{2}\epsilon_4^2 \cos 8\phi. \tag{5.6}$$

The rod is smooth for $-1/18 \le \epsilon_4 \le 1/12$.

For this orientation, $\gamma_{\theta\phi}(\phi, \pi/2)$ vanishes, leading to a decoupling of (3.27), (3.28) that leaves a single equation,

$$\frac{\partial H_n}{\partial_{\phi\phi}} + \left(1 - k^2\left[1 + \epsilon_4 A_1(\phi) + \epsilon_4^2 A_2(\phi)\right]\right) H_n = \mu_n H_n, \tag{5.7}$$

where

$$A_1 = -6[1 + 3\cos 4\phi], \quad A_2 = -\frac{9}{2}[1 - 28\cos 4\phi - 5\cos 8\phi]. \tag{5.8}$$

For the asymptotics, we assume a symmetry condition about $\phi = \pi/2$. If $-\pi/2 \le \psi_R \le \pi/2$, then $\psi_L = \pi - \psi_R$. Then the boundary conditions become

$$H_n(\psi_R)\sin\psi_R + H_{n\phi}(\psi_R)\cos\psi_R = 0, \tag{5.9}$$

$$H_{n\phi}(\pi/2) = 0. \tag{5.10}$$

We take the simple expansions of H_n and μ_n in terms of small ϵ_4:

$$H_n(\phi) = H_n^{(0)}(\phi) + \epsilon_4 H_n^{(1)}(\phi) + O\left(\epsilon_4^2\right), \tag{5.11}$$

$$\mu_n = \mu_n^{(0)} + \epsilon_4 \mu_n^{(1)} + O(\epsilon_4^2). \tag{5.12}$$

The formal asymptotic expansion gives

$$H_n(\phi) = C_1 \cos\beta_n(\pi/2 - \phi) + O(\epsilon_4), \tag{5.13}$$

$$\mu_n = 1 - k^2 - \beta_n^2 + \epsilon_4\left\{6k^2 - \frac{9k^2\beta_n}{(\eta_n + \sin\eta_n)}\left[\sin 4\psi_R^{(0)} + \frac{\sin(4\psi_R^{(0)} - \eta_n)}{(\beta_n + 2)} - \frac{\sin(4\psi_R^{(0)} + \eta_n)}{(\beta_n - 2)}\right]\right\} + O(\epsilon_4^2), \tag{5.14}$$

where $\eta_n = 2\beta_n(\pi/2 - \psi_R^{(0)})$ and the value of β_n must satisfy

$$\cos\beta_n(\pi/2 - \psi_R)\sin\psi_R + \beta_n \sin\beta_n(\pi/2 - \psi_R)\cos(\psi_R) = 0.$$

In Figure 5.2, the first two terms of the asymptotic expansion for the most unstable mode, μ_0, are compared against the numerical value for several choices of contact angle, $\psi_R^{(0)}$, for $\epsilon_4 = 0.20$. The asymptotic results, shown by the dashed curves, are

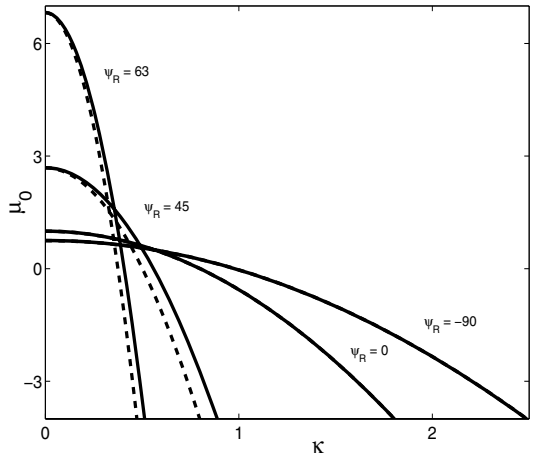

FIG. 5.2. *Eigenvalues for $n = 0$ versus the rescaled wave number $\kappa = R_e k$ for the* [001] *orientation. Reading from the solid lower curve to the solid upper curve at $\kappa = 0$, the corresponding values of ψ_R are $-90, 0, 45, 63$ degrees as indicated. The solid curve represents the numerical solution, and the dashed curve represents the asymptotic solution for $\epsilon_4 = 0.020$.*

close to the numerical results represented by the solid curves. These results show that the larger contact angles are more stable with respect to large dimensionless axial wave numbers. In addition, the [001] orientation is more stable with respect to the isotropic case for negative ϵ_4 and destabilized for positive ϵ_4. The $\psi_R = 0$ case corresponds to the free rod discussed in [10].

The corresponding critical wave number κ_C, defined where μ_0 is zero, as a function of ϵ_4 has the form $\kappa_C = R_e k$. If we define $\sigma_n^{(1)} = k^2\tau$, then the critical dimensionless wave number is as follows:

$$\kappa_C^2 = R_e^2(1 - \beta_n^2)(1 + \epsilon_4\tau) + O(\epsilon_4^2). \tag{5.15}$$

Figure 5.3 shows the results for the square of the rescaled critical wave number versus the contact angle ψ_R. The isotropic case, where ϵ_4 is zero, matches the results found in McCallum et al. [19] for the isotropic rod in contact with a substrate. It is clear from Figure 5.3 that the negative values of ϵ_4 stabilize the rod for all contact angles with respect to the isotropic rod, while the positive values of ϵ_4 destabilize the rod. This behavior also was observed for the freestanding rod [10].

5.2.2. Rod axis parallel to [011] orientation. The dimensionless surface energy, γ, for the [011] orientation is given by (4.15). In the plane $\theta = \pi/2$, we then have $\gamma_{\theta\phi} = 0$, and

$$\gamma = \left(1 + \frac{9}{4}\epsilon_4\right) + \epsilon_4 \cos 2\phi + \frac{3}{4}\epsilon_4 \cos 4\phi, \tag{5.16}$$

(5.17)

$$\begin{aligned}(\gamma + \gamma_{\phi\phi})\,(\gamma + \gamma_{\theta\theta}) = \Big(&1 + \frac{3}{2}\epsilon_4[5 - 12\cos 2\phi - 9\cos 4\phi] \\ &+ \frac{9}{32}\epsilon_4^2[167 + 136\cos 2\phi - 148\cos 4\phi + 312\cos 6\phi + 45\cos 8\phi]\Big).\end{aligned}$$

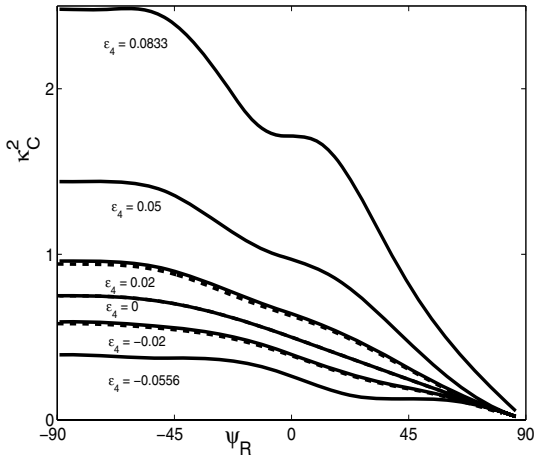

FIG. 5.3. *The square of the critical rescaled wavenumber, κ_C^2, versus ψ_R for the* [001] *orientation for* $\epsilon_4 = -0.0556, -0.02, 0, 0.02, 0.05, 0.0833$. *The solid curves represent the numerical solutions and the dashed curves the asymptotic solutions. The asymptotic solutions are given only for* $\epsilon_4 = -0.02, 0.0.02$.

The asymptotic expansion for the [011] orientation is similar to the [001] orientation. Therefore, we merely state the results for the first two terms of the eigenvalue expansion:

$$\mu_n^{(0)} = 1 - k^2 - \beta_n^2, \tag{5.18}$$

$$\begin{aligned}\mu_n^{(1)} = -\frac{15}{2}k^2 - \frac{9k^2\beta_n}{(\eta_n + \sin\eta_n)}\Bigg[&2\sin 2\psi_R^{(0)} + \frac{3}{4}\sin 4\psi_R^{(0)} \\ &-\left(\frac{2\sin 2\psi_R^{(0)}}{\beta_n^2 - 1} + \frac{3\sin 4\psi_R^{(0)}}{\beta_n^2 - 4}\right)\cos\eta_n \\ &-\left(\frac{2\beta_n\cos 2\psi_R^{(0)}}{\beta_n^2 - 1} + \frac{3\beta_n\cos 4\psi_R^{(0)}}{2(\beta_n^2 - 4)}\right)\sin\eta_n\Bigg],\end{aligned} \tag{5.19}$$

where η_n and β_n are as defined for the [001] orientation. Figure 5.4(a) shows numerical results for the range $-0.05 \le \epsilon_4 \le 0.08$ and the asymptotic results for $\epsilon_4 = -0.02, 0, 0.02$. The extreme ends of the smooth ϵ_4 range present some numerical difficulties and are therefore not shown. Likewise the extreme case, where ψ_R is approaching 90 degrees and the cross-sectional area of the rod is approaching zero, prevents us from calculating over the entire range of ψ_R. The curve $\epsilon_4 = 0$ corresponds to the isotropic case. The substrate acts as a stabilizing influence on the rod; even the negative ϵ_4 case, while less stable than the positive ϵ_4 case, is less unstable than it is for a freestanding rod. The large wave number instability associated with negative values of $(\gamma + \gamma_{\theta\theta})$ seen in the freestanding rod [10] when ϵ_4 is in the range $-5/68 \le \epsilon_4 \le -1/18$ is possibly related to the growing κ_C^2 values observed for $\epsilon_4 = -0.05$ over a positive range of ψ_R.

5.2.3. Rod axis parallel to [111] orientation. If the axis of the rod is aligned with the [111] orientation of the crystal axes relative to the rod axis, then γ is given by the following in the plane $\theta = \pi/2$:

$$\gamma = 1 + 2\epsilon_4, \tag{5.20}$$

$$(\gamma + \gamma_{\phi\phi})(\gamma + \gamma_{\theta\theta}) = 1 + 12\epsilon_4 + 20\epsilon_4^2. \tag{5.21}$$

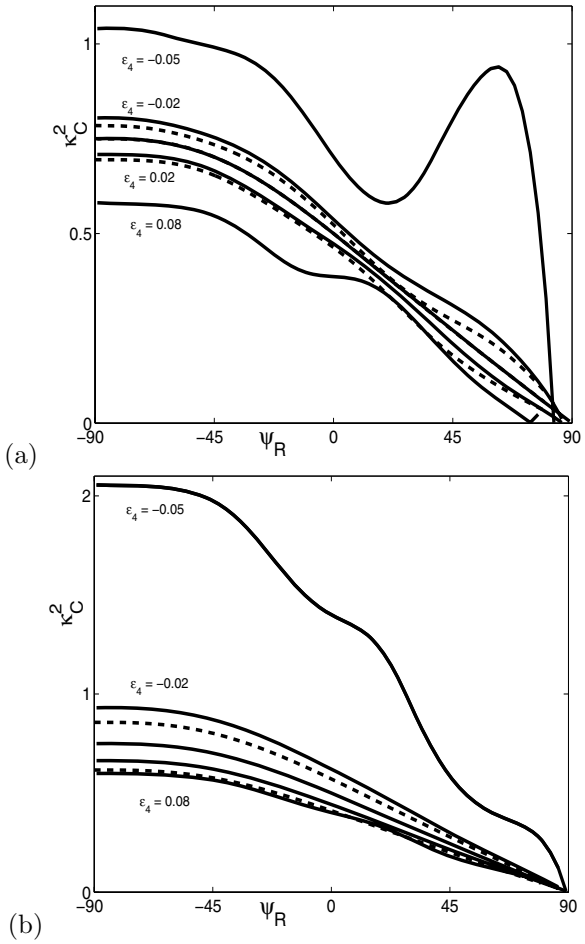

FIG. 5.4. *The square of the critical rescaled wave number, κ_C^2, versus ψ_R for $\epsilon_4 = -0.05, -0.02, 0, 0.02, 0.08$ for* (a) *the* [011] *orientation and* (b) *the* [111] *orientation. The solid curves represent the numerical solutions, and the dashed curves represent the asymptotic solutions. The asymptotic solutions are given only for $\epsilon_4 = -0.02, 0.0.02$.*

The asymptotic expansion for this orientation differs from the expansions for the [001] and [011] orientations since in the [111] orientation (3.27) and (3.28) are coupled through the nonzero term

$$\gamma_{\theta\phi} = 8\sqrt{2}\epsilon_4 \sin 3\phi. \tag{5.22}$$

The zeroth-order conditions and results are the same as those for the [001] and [011] orientations, as expected, so only the details for the first-order terms are shown here. We begin with the equations that must be solved to determine $\mu_n^{(1)}$:

$$\begin{aligned} &- H_{n\phi}^{(1)}(\psi_0)u(\psi_0) + H_n^{(1)}(\psi_0)u_\phi(\psi_0) \\ &- \int_{\psi_R^{(0)}}^{\pi/2} [(\mu_n^{(1)} + 12k^2)H_n^{(0)} - k\gamma_{\theta\phi}(\phi)G_{n\phi}^{(0)} - k(\gamma_{\theta\phi}(\phi)G_n^{(0)})_\phi]u\, d\phi = 0 \end{aligned} \tag{5.23}$$

and

$$-G^{(1)}_{n\phi}(\psi^{(0)}_R)u(\psi^{(0)}_R)+G^{(1)}_{n}(\psi^{(0)}_R)u_\phi(\psi^{(0)}_R) - \int_{\psi^{(0)}_R}^{\pi/2}[(\mu^{(1)}_n+12k^2)G^{(0)}_n+k\gamma_{\theta\phi}(\phi)H^{(0)}_{n\phi}+k(\gamma_{\theta\phi}(\phi)H^{(0)}_n)_\phi]u\,d\phi=0 \tag{5.24}$$

with the boundary conditions

$$H^{(1)}_{n\phi}(\pi/2)=0, \tag{5.25}$$

$$G^{(1)}_{n\phi}(\pi/2)=0, \tag{5.26}$$

$$H^{(1)}_n(\psi^{(0)}_R)\sin\psi^{(0)}_R+H^{(1)}_{n\phi}(\psi^{(0)}_R)\cos\psi^{(0)}_R+k\gamma_{\theta\phi}(\psi^{(0)}_R)G^{(0)}_n\cos\psi^{(0)}_R=0, \tag{5.27}$$

$$G^{(1)}_n(\psi^{(0)}_R)\sin\psi^{(0)}_R+G^{(1)}_{n\phi}(\psi^{(0)}_R)\cos\psi^{(0)}_R-k\gamma_{\theta\phi}(\psi^{(0)}_R)H^{(0)}_n\cos\psi^{(0)}_R=0. \tag{5.28}$$

Concentrating on (5.23), one sees that the equation can be rewritten as

$$-\big(H^{(1)}_{n\phi}(\psi^{(0)}_R)+k\gamma_{\theta\phi}(\psi^{(0)}_R)G^{(0)}_n(\psi^{(0)}_R)\big)u(\psi^{(0)}_R)+H^{(1)}_n(\psi^{(0)}_R)u_\phi(\psi^{(0)}_R) -(\mu^{(1)}_n+12k^2)\int_{\psi^{(0)}_R}^{\pi/2}H^{(0)}_n u\,d\phi+k\int_{\psi^{(0)}_R}^{\pi/2}[\gamma_{\theta\phi}(\phi)G^{(0)}_{n\phi}u(\phi)-\gamma_{\theta\phi}(\phi)G^{(0)}_n u_\phi(\phi)]\,d\phi=0. \tag{5.29}$$

The boundary terms vanish since the operator is self-adjoint. In addition, since $G^{(0)}_n(\phi)$ and $u(\phi)$ differ only by a constant, the second integral vanishes as well. Thus one finds that

$$\mu^{(1)}_n=-12k^2. \tag{5.30}$$

Applying similar logic to (5.24), one finds the same result.

The numerical results for the [111] orientation for $-0.05\le\epsilon_4\le 0.08$ and the asymptotic results for $\epsilon_4=-0.02,0,0.02$ are shown in Figure 5.4(b). The extreme ends of the smooth ϵ_4 range present some numerical difficulties and are therefore not shown. Figure 5.4(b) shows that for nonnegative ϵ_4, the substrate is a stabilizing presence, but even this added stability is unable to overcome the instability associated with positive values of ϵ_4.

6. Conclusion. We have examined rotation effects and the linear stability of a rod on a substrate, in which the rod has a uniform cross-section given by a two-dimensional equilibrium shape. This work extends our previous treatment of a free-standing rod, where the stability analysis produces an associated eigenvalue problem with periodic boundary conditions. The effect of the rod making contact with the substrate involves instead mixed boundary conditions for the eigenvalue problem. The eigenvalues are determined numerically with asymptotic solutions given for the limiting case of small anisotropy. The eigenproblem is a coupled pair of second-order ordinary differential equations with coefficients that are periodic along the axis of the rod and depend on the second derivatives with respect to the orientation variables. We assumed a weak anisotropic surface energy to eliminate missing orientations on the rod.

As was found in our previous exploration of the freestanding anisotropic rod, the magnitude and the sign of the anisotropy determine the relative stability in comparison to the isotropic case. The overall effect of the substrate is stabilizing to the anisotropic rod. In general, as the contact angle ψ_R tends to 90 degrees, the rod on the substrate becomes more stable, which is analogous to the stability of a

three-dimensional planar film, where the anisotropy is not strong enough to make the problem ill-posed. In particular, the rod on a substrate with any of the high symmetry cubic orientations maintains the same relationship as the freestanding rods as to whether or not a positive or negative anisotropy enhances or diminishes stability. When the contact angle ψ_R between the rod and the substrate approaches -90 degrees, the stability does not revert to that of the freestanding rod. In this limiting case, the rods are pinned to the surface at one point, and this single point of contact increases the stability of the rod with respect to the unpinned case. This effect was also seen by McCallum et al. [19] for the isotropic rod.

We have considered the effect of rotation on the stability of a two-dimensional rod whose cross-section is either elliptical or a shape determined by one of the three high symmetry cubic orientations. In order to describe these cross-sections, the coordinate system is fixed to the center of the rod, thereby defining a substrate height above this center. When the major axis of the ellipse is horizontal, the ellipse is most stable with a positive substrate height (see Figure 2.2) and is least stable with a negative substrate height. For this elliptical case, the observation is consistent with the remark above that contact angles near 90 degrees are more stable than contact angles near -90 degrees. But the observation concerning substrate height applies to more general cases. In particular, the stability of rods whose cross-sections are determined by high symmetry cubic orientations mimic this reversal of stability when the substrate height is at a maximum over the coordinate axes in comparison to a minimum. Similar to the linear stability results, the stability under rotation of these rods with the [001] and [011] cubic orientations depends greatly on the sign and magnitude of the anisotropy. Negative anisotropy corresponds to a rod with a cross-section of a rounded cube; positive anisotropy corresponds to a rod with a smoothed octahedral cross-section. In general we observe that for the [001] cubic orientation, the more negative the anisotropy, the more unstable the rod. The situation is reversed for the [011] and [111] cubic orientations.

The two- or fourfold symmetry of the orientations is reflected in the effect of rotation of the rods on the stability. The stability of the rod with the [111] cubic orientation is found to be unchanged by rotation.

These results may be potentially useful in the manufacture of stable long rods or wires with an axis oriented along the high symmetry orientations [001], [011], and [111].

Appendix. The effect of rotations on perturbation stability. In this section we discuss the effect of rotating a crystal on the second variational energy of the contact line problem. We start with a study of the two-dimensional shapes from sections 4.1 and 4.2: an ellipse and three two-dimensional cubic crystals in high symmetry orientations. For the ellipse, the major and minor axes are rotated with respect to the x-axis at an angle of ϕ'. Additionally, the substrate may be moved upwards from the original x-axis at a distance of W_0. In this particular case the effect of W_0 will be seen indirectly, as it does not appear explicitly in the relevant equations. However, W_0 determines the contact angles ψ_R and ψ_L that the crystal makes with the substrate.

In two dimensions the stability problem (i.e., the second variation of the energy) reduces to the following:

$$\frac{E^{(2)}}{2} = -\int_{\psi_R^{(0)}}^{\psi_L^{(0)}} [h_{\phi\phi}(\phi) + h(\phi)]h(\phi)\, d\phi \tag{A.1}$$

with the boundary conditions

$$h(\psi_i^{(0)})\sin\psi_i^{(0)} + h_\phi(\psi_i^{(0)})\cos\psi_i^{(0)} = 0 \tag{A.2}$$

for $i = L, R$, subject to the constraints where

$$\int_{\psi_R^{(0)}}^{\psi_L^{(0)}} h(\phi)\left[\gamma(\phi+\phi') + \gamma_{\phi\phi}(\phi+\phi')\right] d\phi = 0, \tag{A.3}$$

and where

$$\int_{\psi_R^{(0)}}^{\psi_L^{(0)}} h^2(\phi)\, d\phi \tag{A.4}$$

is minimized.

Therefore we can formulate the problem as

$$h_{\phi\phi}(\phi) + h(\phi) = \mu\, h(\phi) + \tau\, \left[\gamma(\phi+\phi') + \gamma_{\phi\phi}(\phi+\phi')\right] \tag{A.5}$$

with the boundary conditions given as above in (A.2). We solve this problem using two different numerical techniques. The first uses a pseudospectral Chebyshev calculation [34] to determine a basis of eigenvectors for the problem

$$h_{\phi\phi}(\phi) + h(\phi) = \mu\, h(\phi), \tag{A.6}$$

subject to the boundary conditions, that are orthogonal to the vector

$$\gamma(\phi+\phi') + \gamma_{\phi\phi}(\phi+\phi'). \tag{A.7}$$

In addition, we can solve (A.2), (A.5) with a double shooting method.

The unstable eigenmodes are those where $\mu_n > 0$. We find that the largest eigenvalue, μ_0, is zero to numerical accuracy for all cases, indicating that none of the modes are unstable. Analytically we can obtain some insight by noting that (A.6) admits solutions of the form

$$-n^2 + 1 = \mu_n, \tag{A.8}$$

$$h_n(\phi) = A_n \sin(n\phi) + B_n \cos(n\phi). \tag{A.9}$$

Note that μ_n is negative for $n \geq 2$, resulting in stable shape perturbations. The boundary conditions show that if $n = 0$, then $h_0 = 0$. The next allowed n is $n = 1$, which gives $\mu_1 = 0$ and $h_1 = B_1 \cos\phi$, an allowable solution. This is an eigenmode as long as it satisfies the orthogonality constraint given in (A.3).

Acknowledgments. The authors are grateful for helpful discussions with D. L. Cotrell.

REFERENCES

[1] M. Asta, J. J. Hoyt, and A. Karma, *Calculation of alloy solid-liquid interfacial free energies from atomic-scale simulations*, Phys. Rev. B, 66 (2002), 100101.

[2] J. W. Cahn, *Stability of rods with anisotropic surface free energy*, Scripta Metall., 13 (1979), pp. 1069–1071.

[3] J. W. Cahn and D. W. Hoffmann, *A vector thermodynamics for anisotropic interfaces*, II. *Curved and facetted surfaces*, Acta Metall., 22 (1974), pp. 1205–1214.
[4] S.-C. Chang, J.-M. Shieh. B-T. Dai, M.-S. Feng, and Y.-H. Li, *The effect of plating current densities on self-annealing behaviors of electroplated copper films*, J. Electrochem. Soc., 149 (2002), G535.
[5] J. S. Chen, B. C. Lim, and J. P. Wang, *Controlling the crystallographic orientation and the axis of magnetic anisotropy in LI(o) FePT films*, Appl. Phys. Lett., 81 (2002), pp. 1848–1850.
[6] J. Diao, K. Gall, and M. L. Dunn, *Surface stress driven reorientation of gold nanowires*, Phys. Rev. B, 70 (2004), 075413.
[7] T. Gao, G. W. Meng, Y. Wang, S. Sun, and J. Zhang, *Electrochemical synthesis of copper nanowires*, J. Phys. Condens. Matter, 14 (2002), pp. 355–363.
[8] T. Gao, G. W. Meng, J. Zhang, Y. W. Wang, C. H. Liang, J. C. Fan, and L. D. Zhang, *Template synthesis of single-crystal Cu nanowire arrays by electrodeposition*, Appl. Phys. A, 73 (2001), pp. 251–254.
[9] A. M. Glaeser, *A new approach to investigating surface transport in ceramics,* in Mass and Charge Transport in Ceramics, K. Koumoto, H. Matsubara, and L. M. Sheppard, eds., Ceramic Trans. 71, American Ceramic Society, Westerville, OH 1996, pp. 117–136.
[10] K. F. Gurski and G. B. McFadden, *The effect of anisotropic surface energy on the Raleigh instability*, R. Soc. Cond. Proc. Ser. A Math. Phys. Eng. Sci., 459 (2003), pp. 2575–2598.
[11] J. M. E. Harper, C. Cabral, Jr., P. C. Andricacos, L. Gignac, I. C. Noyan, K. P. Rodbell, and C. K. Hu, *Mechanisms for microstructure evolution in electroplated copper thin films near room temperature*, J. Appl. Phys., 86 (1999), pp. 2516–2525.
[12] C. Herring, *The use of classical macroscopic concepts in surface-energy problems*, in Structure and Properties of Solid Surfaces, R. Gomer and C. S. Smith, eds., University of Chicago Press, Chicago, 1953, pp. 5–72.
[13] D. W. Hoffmann and J. W. Cahn, *A vector thermodynamics for anisotropic interfaces*. I. *Fundamentals and applications to plane surface junctions*, Surf. Sci., 31 (1972), pp. 368–388.
[14] J. J. Hoyt, M. Asta, and A. Karma, *Method for computing the anisotropy of the solid-liquid interfacial free energy*, Phys. Rev. Lett., 86 (2001), pp. 5530–5533.
[15] H. H. Huang, M. H. Hon, and M. C., Wang, *Effect of NH3 on the growth characterization of TiN films at low temperature*, J. Crystal Growth, 240 (2002), pp. 513–520.
[16] D. A. Kessler and H. Levine, *Growth velocity of three-dimensional dendritic crystals*, Phys. Rev. A, 36 (1987), pp. 4123–4126.
[17] D. A. Kessler and H. Levine, *Pattern selection in three dimensional dendritic growth*, Acta Metall., 36 (1988), pp. 2693–2706.
[18] Y. Kondo and K. Takayanagi, *Gold nanobridge stabilized by surface structure*, Phys. Rev. Lett., 79 (1997), pp. 3455–3458.
[19] M. S. McCallum, P. W. Voorhees, M. J. Miksis, S. H. Davis, and H. Wong, *Capillary instabilities in solid thin films: Lines*, J. Appl. Phys., 79 (1996), pp. 7604–7611.
[20] G. B. McFadden, S. R. Coriell, and R. F. Sekerka, *Effect of surface tension anisotropy on cellular morphologies*, J. Crystal Growth, 91 (1988), pp. 180–198.
[21] G. B. McFadden, S. R. Coriell, and R. F. Sekerka, *Effect of surface free energy anisotropy on dendrite tip shape*, Acta Mater., 48 (2000), pp. 3177–3181.
[22] D. H. Michael, *Meniscus stability*, Ann. Rev. Fluid Mech., 13 (1981), pp. 189–215.
[23] M. E. Toimil Molares, A. G. Balogh, T. W. Cornelius, R. Neumann, and C. Trautmann, *Fragmentation of nanowires driven by Rayleigh instability*, Appl. Phys. Lett., 85 (2004), pp. 5337–5339.
[24] M. E. Toimil Molares, J. Brötz, V. Buschmann, D. Dobrev, R. Neumann, R. Scholz, I. U. Schuchert, C. Trautmann, and J. Vetter, *Etched heavy ion tracks in polycarbonate as template for copper nanowires*, Nucl. Instrum. Methods Phys. Res. B, 185 (2001), pp. 192–197.
[25] W. W. Mullins, *Solid surface morphologies governed by capillarity*, in Metal Surfaces: Structure, Energetics, and Kinetics, ASM, Metals Park, OH, 1963, pp. 17–66.
[26] Y. T. Pang, G. W. Meng, Y. Zhang, Q. Fang, and L. D. Zhang, *Copper nanowire arrays for infrared polarizer,* Appl. Phys. A, 76 (2003), pp. 533–536.
[27] J. A. F. Plateau, *Experimental and theoretical researches on the figures of equilibrium of a liquid mass withdrawn from the action of gravity*, Annual Reports of the Smithsonian Institution (1863–1866), 1873, pp. 270–285.
[28] Lord Rayleigh, *On the instabilities of jets*, Proc. Lond. Math. Soc., 10 (1878), pp. 4–13.

[29] G. Riveros, H. Gómez, A. Cortes, R. E. Marotti, and E. A. Dalchiele, *Crystallographically-oriented single-crystalline copper nanowire arrays electrochemically grown into nanoporous anodic templates*, Appl. Phys. A, 81 (2005), pp. 17–24.

[30] C. Rottman and M. Wortis, *Statistical mechanics of equilibrium crystal shapes: Interfacial phase diagrams and phase transitions*, Phys. Rep., 103 (1984), pp. 59–79.

[31] R. V. Roy and L. W. Schwartz, *On the stability of liquid ridges*, J. Fluid Mech., 391 (1999), pp. 293–318.

[32] J. S. Stölken and A. M. Glaeser, *The morphological evolution of cylindrical rods with anisotropic surface free energy via surface diffusion*, Scripta Metall. Mater., 27 (1992), pp. 449–453.

[33] J. E. Taylor, *Mean curvature and weighted mean curvature*, Acta Metall. Mater., 40 (1992), pp. 1475–1485.

[34] R. G. Voigt, D. Gottlieb, and M. Y. Hussaini, *Spectral Methods for Partial Differential Equations*, SIAM, Philadelphia, 1984.

[35] P. W. Voorhees, S. R. Coriell, G. B. McFadden, and R. F. Sekerka, *The effect of anisotropic crystal-melt surface tension on grain boundary groove morphology*, J. Crystal Growth, 67 (1984), pp. 425–440.

[36] W. L. Winterbottom, *Equilibrium shape of a small particle in contact with a foreign substrate*, Acta Metall., 15 (1967), pp. 303–310.